Springer

KSME

Journal of Mechanical Science and Technology 32 (1) (2018) 223~229
www.springerlink.com/content/1738-494x(Print)/1976-3824(Online)
DOI 10.1007/s12206-017-1223-9

Progressive failure of metal–composite hybrid wheels under impact †

Shun-Fa Hwang[1,*], Hui-Lun Yu[1], Yu-Jen Liu[1], Yuder Chen[2], Shih-Chieh Chen[3] and Yueh-Chih Hsieh[3]

[1]*Department of Mechanical Engineering, National Yunlin University of Science and Technology, 123 University Road, Sec. 3, Douliu, Yunlin 64002, Taiwan, ROC*
[2]*Chung-Shan Institute of Science and Technology, P.O. Box 90008-11-3, Taichung 40722, Taiwan, ROC*
[3]*Hocheng Corporation, No. 135, Hou-Chung St., Bade Dist., Taoyang 33443, Taiwan, ROC*

(Manuscript Received April 10, 2017; Revised October 2, 2017; Accepted October 19, 2017)

Abstract

An 18-in hybrid wheel consisting of an aluminum alloy disk and a composite rim under 13° impact test is considered in this study. The rim is made of carbon fabric/polyurethane composites fabricated by resin transfer molding. Explicit finite element analysis with progressive failure function is used to investigate the failure situation of the hybrid wheel and the suitable braid angle of the braided composite. The effective elastic constants and strengths of the braided composites predicted by basic finite element analyses are adopted, whereas the true stress–strain curve of aluminum is used for the disk. Simulation results indicate that the aluminum alloy disk is safe after the impact test, whereas the rim is damaged. The volume of failed elements after impact simulation is selected as an indicator to obtain a quantity that can be used to represent the damage situation of the rim. Compared with the test results of a real hybrid wheel with [±30°] fiber angle in the rim, the hybrid wheel with fiber angle in the rim that is greater than [±30°] could pass the impact test.

Keywords: Hybrid wheel; Braided composite; Impact test; Progressive failure; Finite element analysis

1. Introduction

Wheels are one of the most important components in the automotive industry because they have a strong influence on the safety, stability, and economy of vehicles. Making wheels from lightweight metal, for example, aluminum alloy due to its excellent lightness and corrosion resistance, is recently popular to reduce the weight and increase the fuel efficiency. With these requirements, wheel manufacturers have been focusing increasing attention to lightweight designs by new materials and manufacturing technologies. Polymer matrix composites are suitable candidate to fulfill these requirements because of their high specific stiffness, high specific strength, excellent corrosion resistance, and good fatigue property. Given that the specific weight of advanced polymer composites is lower than that of aluminum alloy, the weight of a vehicle can be further reduced if advanced composite materials are used to replace aluminum alloy for wheels. Several examples using composite materials for wheels could be found in certain websites [1, 2].

Traditionally, composite structures are fabricated by the layup processes. However, the long fabrication time and intensive labor hours are always disadvantages. Resin transfer molding (RTM) is one viable alternative, in which the fiber is made into fabric in advance and the resin is injected subsequently to avoid these disadvantages. Through this process, the composite structures could have complicated shapes and could be fabricated in a short time. In RTM, epoxy is commonly used because of its good mechanical properties. However, solvents, which may harm human beings and the environment, are often added to epoxy to reduce its viscosity and increase its flowability. Recently, one type of Polyurethane (PU) has been developed without the need to add solvents, and it has low viscosity, good mechanical properties, and high transition temperature. Thus, this type of PU is suitable for the RTM.

Wheels need to pass strict requirements before use because they have key effects on passenger safety. From the standard, bending fatigue test, radial fatigue test, and impact test are the three main wheel tests. The bending fatigue test applies a constant rotating bending moment to the wheel to simulate the cornering-induced loads. In the radial fatigue test, a radial load is applied by a constantly rotating drum on the wheel–tire assembly. The impact test is conducted to evaluate the impact damage of the wheel by dropping a striker. Generally, making a new wheel to pass all these three tests is highly time consuming because it takes time to manufacture, test, and inspect a wheel, and this process is repeated several times. Finite element analysis is generally adopted to reduce the time spent in

*Corresponding author. Tel.: +886 5 5342601 Ext. 4143, Fax.: +886 5 5312062
E-mail address: hwangsf@yuntech.edu.tw
† Recommended by Associate Editor Kyeongsik Woo

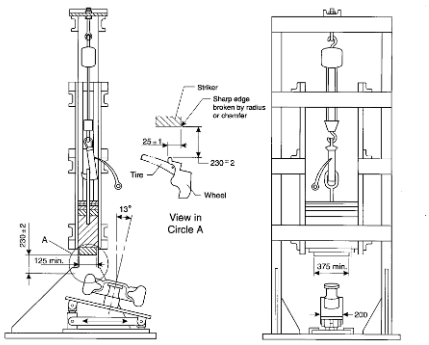

Fig. 1. Impact loading test machine [11].

trial and error during the development and testing phases. In the literature, numerous works using finite element analysis to predict the possible failure of a new style of metal wheel and even to optimize the metal wheel shape have been reported [3-5]. Among the three tests, the impact test is always considered for finite element analysis because of its highly dynamic behavior and quick test. For example, Merit [6] used 3-D explicit finite element methods to simulate the impact test of cast aluminum alloy wheel and showed that the maximum von Mises stress occurs at the lug region. Chang and Yang [7] used nonlinear dynamic finite element analysis to simulate the impact test of forged aluminum alloy wheel. Their simulation results indicated that the total plastic work could be effectively employed as a fracture criterion for forged aluminum alloy wheels during the impact test. The equivalent plastic strain [8, 9] was used as a damage indicator to determine whether the wheel passed or failed the impact test, and the correlation between the experimental result and the numerical prediction was good. For composite materials, Bae et al. [10] inserted a friction damping layer between composite and aluminum alloy parts of a rim to enhance the damping capacity and ride comfort, and their experimental tests proved that this new wheel could pass the three tests and reduce the noise.

A hybrid wheel consisting of an aluminum alloy disk and a composite rim is considered in this study to progressively apply composite materials in wheels. The rim is made of carbon fabric/PU composites fabricated by RTM. Explicit finite element analysis with progressive failure function is used to investigate the failure situation of this hybrid wheel under the 13° impact test. Therefore, the braid angle of the braided composite could be appropriately selected to pass the impact test.

2. Testing standard

Wheel impact test is conducted to simulate the situation that the wheel collides with the curb of the road or a large obstacle. As shown schematically in Fig. 1, this test is executed by dropping a striker with a specific weight from a specific height to hit the wheel–tire assembly. According to the impact test standard [11], the wheel–tire assembly is mounted at an angle of 13° to the horizontal plane, and its highest point is under the striker. For a wheel with the diameter of 18 in., the mass of the striker is 594 kg, and its impacting surface is at least 125 mm wide and 230 mm long. Before the impact, the height of the striker is 230 ± 2 mm above the highest point of the rim flange. The striker will hit the tire and the rim, and the striker edge will overlap the rim flange by 25 mm. Before the test, the tire is inflated to a pressure of 200 ± 10 kPa.

To pass the regulation of the test standard, the tested wheel must satisfy the following minimum performance standards [11]: No visible fracture of the central member of the wheel assembly, no separation of the central member from the rim, and no sudden loss of tire air pressure. Deformation of the wheel assembly or fracture in the rim section does not constitute a failure.

Table 1. Mechanical properties of aluminum 6061-T6.

Young's modulus (GPa)	68
Ultimate tensile strength (MPa)	310
Yield tensile strength (MPa)	280
Density (g/cm^3)	2.7
Poisson ratio	0.33

Fig. 2. Hybrid wheel with aluminum alloy disk and composite rim.

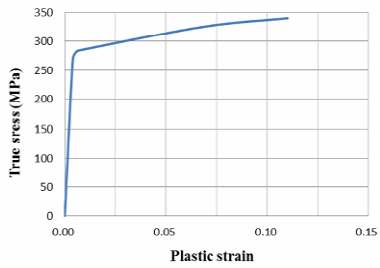

Fig. 3. True stress–strain relationship of aluminum alloy 6061-T6.

3. Material properties

The 18-in hybrid wheel consisting of an aluminum alloy disk and a composite rim is shown in Fig. 2. The mechanical properties of aluminum alloy 6061-T6 are listed in Table 1, and its true stress–strain relationship is shown in Fig. 3. The rim is made of carbon fabric/PU composites fabricated by RTM. Given that the rim is made of braided composites, the braid angle is an important factor that affects the mechanical

Table 2. Mechanical properties of unidirectional carbon/PU composite.

E_1 (GPa)	124.44
E_2 (GPa)	9.63
v	0.243
G (GPa)	7.81
X_t (GPa)	1.288
X_c (GPa)	0.23
Y_t (GPa)	0.058
Y_c (GPa)	0.161
S (GPa)	0.076

Table 3. Comparison of predicted and measured strengths of braided composites.

Braided composite	X_{tm} (GPa)	X_{tp} (GPa)	X_{cm} (GPa)	X_{cp} (GPa)
[0/90/90/0]	0.748	0.720 (−3.8 %)	0.127	0.130 (2.0 %)
[17.5/−17.5/−17.5/17.5]	0.837	0.869 (3.9 %)	0.168	0.185 (9.8 %)
[21.5/−21.5/−21.5/21.5]	0.657	0.706 (7.5 %)	0.152	0.166 (9.1 %)
[25/−25/−25/25]	0.544	0.576 (5.8 %)	0.149	0.151 (1.7 %)

properties of the rim and ensures that it passes the impact test. However, obtaining the mechanical properties of braided composites with different braid angles is cumbersome. Therefore, an easy method should be employed to predict the effective elastic constants and strengths of the braided composites, such that these properties could be used in finite element analysis to evaluate their performance under dynamic impact.

According to the ASTM standard, the measured elastic constants and strengths of unidirectional carbon/PU composites are shown in Table 2. The Young's modulus, Poisson's ratio, and shear modulus are denoted as E, v and G, respectively. The longitudinal, transverse, and shear strengths are expressed as X, Y and S, respectively. The subscript 1 denotes the fiber direction, and the subscript 2 denotes the direction perpendicular to the fiber direction. The subscript t represents tension, and the subscript c represents compression. In this composite, the fiber used is TAIRYFIL TC-36S with the specification of 12 K made by Formosa Plastics Corporation, and the resin provided by Huntsman Ltd. is composed of EID 9931 resin and VITROX RTM 00180 polyol blend with the weight ratio of 92:8. Before the injection, the resin is vacuumed for 40 min to evacuate possible bubbles. After the injection, the specimen is maintained at 120 °C for 60 min for curing.

In this work, the effective elastic constants and strengths of the braided composites are estimated from the properties of unidirectional carbon/PU composites by basic finite element analyses [12]. In these finite element analyses, two braided carbon/PU layers are considered, with each braided layer treated as two unidirectional layers, and symmetric layup is enforced. The Tsai–Wu criterion has been applied to calculate

Table 4. Mechanical properties of braided composite.

Fiber angle	[±20°]	[±30°]	[±45°]	[±60°]	[±70°]
E_1 (GPa)	89.17	55.88	25.51	14.38	11.41
E_2 (GPa)	11.41	14.38	25.51	55.88	89.17
v	0.967	1.043	0.632	0.268	0.123
G (GPa)	18	26.32	32.38	26.32	18
X_t (GPa)	0.766	0.423	0.175	0.092	0.071
X_c (GPa)	0.174	0.143	0.139	0.132	0.146
Y_t (GPa)	0.071	0.092	0.175	0.423	0.766
Y_c (GPa)	0.146	0.132	0.139	0.143	0.174
S (GPa)	0.296	0.453	0.656	0.453	0.297

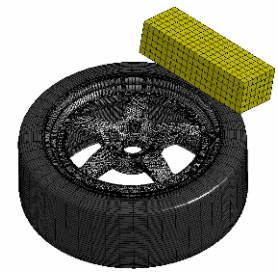

Fig. 4. The meshed wheel–tire assembly and striker.

the effective strengths of the braided composite. For Young's modulus, the predicted values have less than 7.6 % difference with the experimental results for different braid angles [12]. For Poisson's ratio, the difference is slightly higher by up to 18.6 %. Table 3 shows that, for the longitudinal tensile strength X_t and the longitudinal compressive strength X_c, the second subscript m represents the measured value and p denotes the predicted value. For the braided composites, the maximum difference between measured and predicted strengths is approximately 7.5 % and 9.8 % for tensile and compressive strengths, respectively. Therefore, the use of the effective mechanical properties of braided composites may be verified.

Upon using the properties of unidirectional carbon/PU composites, the effective properties of braided composites for the braid angles of 40°, 60°, 90°, 120° and 140° are predicted and shown in Table 4. In this table, the fiber angles are shown for each braided composite layer, and the braid angle should sum up the fiber angle. For example, the fiber angle [±30°] represents the braid angle of 60°. In this table, E_1 and E_2 are the longitudinal and transverse Young's moduli, respectively. These effective properties will be used in the subsequent finite element analyses for dynamic impact.

4. Finite element analysis

For dynamic impact analysis, an explicit finite element package, that is, LS-DYNA, is selected. HyperMesh is used to mesh the hybrid wheel, and the meshed wheel–tire assembly

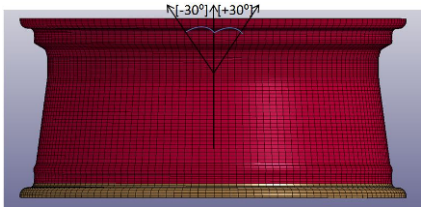

Fig. 5. Fiber angle of braided composite for the rim.

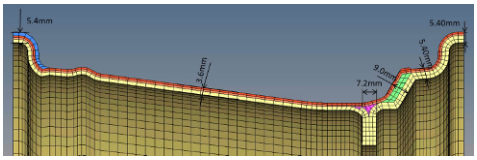

Fig. 6. Thickness and mesh along the thickness direction of the rim.

and striker are shown in Fig. 4. Eight-node hexahedral solid elements are used for the striker, tire, and rim. These three parts have a total of 69450 elements and 90575 nodes. For the aluminum alloy disk, four-node tetrahedral solid elements are used, and it has a total of 63400 elements and 17636 nodes. Although effective properties have been used for the braided composites, the longitudinal direction of the composite rim that is along the axial direction should be specified, as shown in Fig. 5. The fiber directions of the composite with the braid angle of 60° are also shown in the figure. The thickness of the rim varies along the axial direction, as shown in Fig. 6; as such, the thickness variation should be carefully handled.

The striker with the velocity of 2.006 m/s is released from the height of 25 mm above the highest point of the wheel assembly to simplify the simulation model for the impact test. This velocity is calculated from the original height of 230 mm. For the boundary conditions, the mounting surface of the hub is fully fixed. The striker is modeled as a rigid body by the material model MAT20 of LS-DYNA with the Young's modulus of 210 GPa, Poisson's ratio of 0.3, and density of 1.267 g/cm^3. The tire is treated as rubber by the material model MAT1 with the Young's modulus of 2.54 GPa, Poisson's ratio of 0.33, and density of 1.11 g/cm^3. Before the impact, the tire is inflated with 200 kPa air pressure. The nonlinear elastic–plastic material model is used to describe the behavior of the aluminum alloy disk. The true stresses and plastic strains are used to plot the curve, as shown in Fig. 3, and this curve is directly imported to LS-DYNA. The material model is MAT24 with the properties listed in Table 1.

The material model, MAT54, with the progressive failure function is used to describe the behavior of the braided composite. The mechanical properties used are listed in Table 4. The progressive failure function allows some of the materials to fail during the impact process. To achieve this, the Chang–Chang failure criterion is selected to determine the failure of each layer.

Tensile failure in the longitudinal direction is expressed as:

$$e_{f,t}^2 = \left(\frac{\sigma_{11}}{X_t}\right)^2 + \beta\left(\frac{\sigma_{12}}{S}\right)^2 - 1 \geq 0 . \quad (1)$$

Compressive failure in the longitudinal direction is expressed as:

$$e_{f,c}^2 = \left(\frac{\sigma_{11}}{X_c}\right)^2 - 1 \geq 0 . \quad (2)$$

Tensile failure in the transverse direction is expressed as:

$$e_{m,t}^2 = \left(\frac{\sigma_{22}}{Y_t}\right)^2 + \left(\frac{\sigma_{12}}{S}\right)^2 - 1 \geq 0 . \quad (3)$$

Compressive failure in the transverse direction is expressed as:

$$e_{m,c}^2 = \left(\frac{\sigma_{22}}{2S}\right)^2 + \frac{\sigma_{22}}{Y_c}\left(\frac{Y_c^2}{4S^2} - 1\right) + \left(\frac{\sigma_{12}}{S}\right)^2 - 1 \geq 0 . \quad (4)$$

In the equations, X_t and X_c are the tensile and compressive strengths of the braided composite along the longitudinal (Axial) direction, respectively; Y_t and Y_c are the tensile and compressive strengths of the braided composite along the transverse (Hoop) direction, respectively; and S is the shear strength. For stress, the index 1 denotes the longitudinal (Axial) direction and the index 2 represents the transverse (Hoop) direction. The coefficient β could be used to scale the shear stress effect on the tensile failure in the longitudinal direction. In this study, $\beta = 0$ is used and yields the simple maximum stress criterion without interaction.

Damage occurs if one of the four criteria is met. In addition to these stress-based criteria, failure strains can be also specified. When the failure strains are specified, after satisfying the Chang–Chang criterion, the stress level is kept at a constant level until the failure strains are fulfilled. Then, the stiffness properties of this layer become zero. Given that each element has only one layer, the element fails and disappears as its layer fails.

5. Results and discussion

The aluminum alloy disk is selected because it passed the impact test for an all-aluminum alloy wheel. Therefore, the function of progressive failure is only activated for the composite rim and deactivated for the aluminum alloy disk to simplify the simulation of the hybrid wheel under the impact test. However, the plastic work is also used as an index to evaluate the possibility of damage and to assess the safety of the disk. The plastic work w is defined as:

$$w = \int_0^{\varepsilon_f} \sigma_t d\varepsilon_p , \quad (5)$$

Table 5. Plastic work of aluminum disk with composite rim of different fiber angles.

Fiber angle	Plastic work (Nm/mm^3)
[±20°]	8.605
[±30°]	8.417
[±45°]	7.856
[±60°]	10.133
[±70°]	10.895

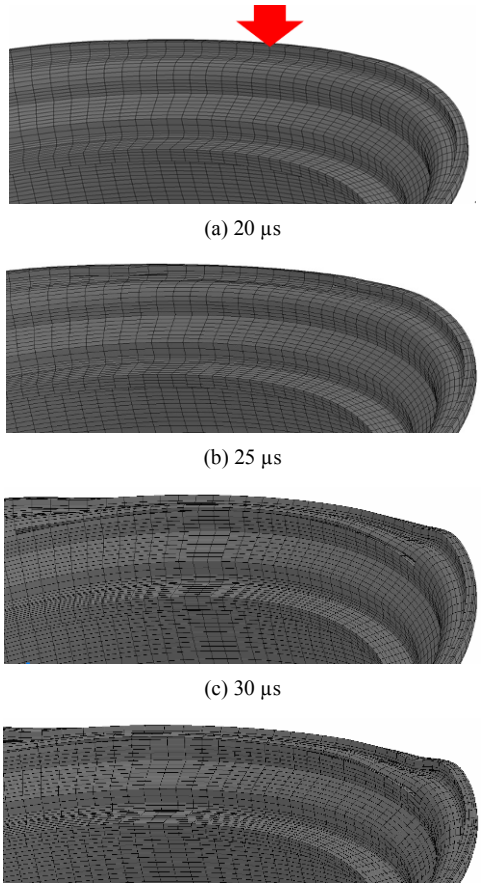

(a) 20 μs

(b) 25 μs

(c) 30 μs

(d) 35 μs

Fig. 7. Snapshots during the impact simulation for the fiber angle of [±30°].

where σ_t denotes the true stress, ε_p represents the plastic strain, and ε_f is the fracture strain. The true stress–strain relationship for the aluminum alloy can be expressed as:

$$\sigma_t = k\left(\varepsilon_p\right)^n, \tag{6}$$

where n is the strain-hardening exponent and k is the strength coefficient. From this equation, the critical strain energy density w_c can be calculated as:

$$w_c = \int_0^{\varepsilon_f} \sigma_t d\varepsilon_p = \frac{\sigma_f \varepsilon_f}{1+n}, \tag{7}$$

Table 6. Damage volume of the composite rim.

Fiber angle	Damage volume (mm^3)
[±20°]	9784.40
[±30°]	9280.60
[±45°]	9256.60
[±60°]	8666.00
[±70°]	8273.10

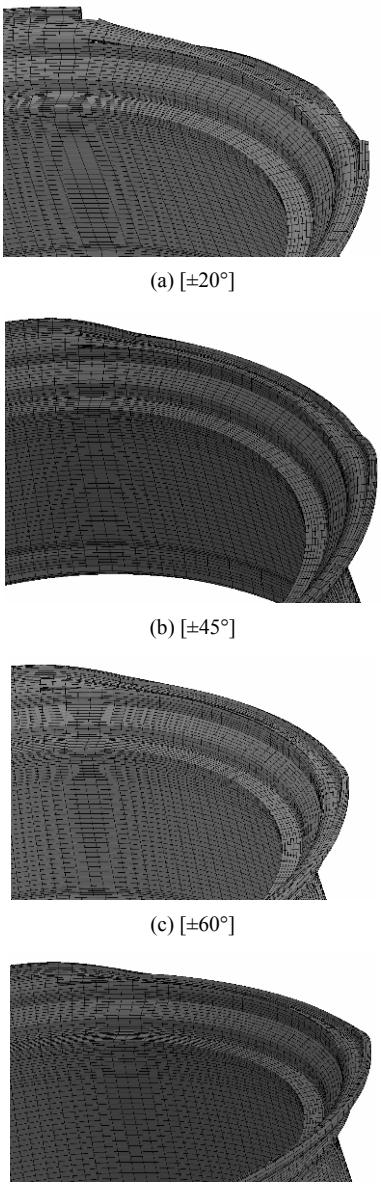

(a) [±20°]

(b) [±45°]

(c) [±60°]

(d) [±70°]

Fig. 8. Final damage situation for different fiber angles.

where σ_f is the true fracture stress. From Fig. 3, the obtained critical strain energy density w_c is 33.87 Nm/mm^3. From the finite element analysis of the impact test, the calculated plastic work of the aluminum alloy disk with the com-

Fig. 9. Real damage situation of a hybrid wheel of fiber angle [±30°] after the impact test.

posite rim of different braid angles is shown in Table 5. The plastic work of the aluminum alloy disk is from 7.86 Nm/mm^3 to 10.90 Nm/mm^3 and less than the critical strain energy density. Thus, the aluminum alloy disk should be safe after the impact test. In this table, the plastic work initially decreases and subsequently increases as the braid angle of braided composites increases. The plastic work is significantly affected by the mechanical properties of the braided composites because the aluminum alloy disk is supported by the composite rim.

Given that the aluminum alloy disk is safe after the impact test, the major concern is the composite rim with different fiber angles. The progressive failure function is activated for the composite rim, and the damage evolution processes could be determined from the snapshots during the impact simulation, as shown in Fig. 7 for the fiber angle of [±30°]. The other parts, including the striker, tire, and disk are removed from the figures to have a clear view of the damage of the rim. In Fig. 7(a), the red arrow indicates the position of the striker and the time is 20 ms, which is just before the occurrence of damage. At 25 ms, two line cracks appear, as shown in Fig. 7(b). In addition to the slight extension of the previous two line cracks, a long line crack appears at 30 ms, as shown in Fig. 7(c). At 35 ms, which is the end of the impact process, all cracks slightly extend, as shown in Fig. 7(d). The final damage situation for the other fiber angles is shown in Figs. 8(a)-(d). The volume of the failed elements after the impact simulation is calculated to obtain a quantity that can be used to represent the damage situation of the rim. The results are shown in Table 6. The total volume of the composite rim is 1820104.5 mm^3. For these cases, the damage volume is only approximately 4 % to 6 % of the total volume of the rim. The table shows that, as the fiber angle increases, the damage volume is reduced. This finding indicates that the possibility of the composite rim to pass the impact test increases with the increase in the fiber angle.

One aluminum alloy–composite hybrid wheel with [±30°] fiber angle in the rim has been fabricated and tested under 13° impact test. The real damage situation of the impacted region is shown in Fig. 9. According to the regulation, this wheel passes the impact test. The comparison between Figs. 9 and 7(d) shows that they have similar damage situation. Given that this hybrid wheel with [±30°] fiber angle in the rim passes the test, we could infer that the hybrid wheel with fiber angle in the rim that is greater than [±30°] could pass the impact test.

The results indicate the need to replace the aluminum alloy with the composite materials in the rim. However, given that the present study only concentrates on the 13° impact test, we do not infer that the wheel passes the bending and radial fatigue tests because these two tests have different requirements for the wheel. From our preliminary tests, if the composite rim is further improved, then we can expect that this metal–composite hybrid wheel could pass all three tests.

6. Conclusions

Finite element analysis with progressive failure function is established, and the effective elastic constants and strengths of braided composites are used to investigate the suitable braid angle of braided composites used in a rim of a hybrid wheel for 13° impact test. The true stress–strain curve of aluminum alloy is used for the disk, and the plastic work is used as damage indicator. The simulation results indicate that the aluminum alloy disk is safe after the impact test, even though different braid angles are used in the composite rim. The damage revolution of the composite rim could be clearly observed from the simulation, and its damage volume is selected as an indicator. Compared with the test results of a real hybrid wheel with [±30°] fiber angle in the rim, the hybrid wheel with fiber angle in the rim that is greater than [±30°] could pass the impact test.

Acknowledgment

The financial support from Hocheng Corporation and the Ministry of Economic Affairs, Taiwan, through 103-EC-17-A-08-12-007, is gratefully acknowledged.

References

[1] *http://www.wheelsandmore.de/en/Tuning/Aston-Martin-Vanquish/ Vanquish.html*.

[2] *http://www.roadandtrack.com/car-culture/videos/a7653/making-the-koenigsegg-one-1-wheel/*.

[3] H. M. Karandikar and W. Fuchs, Fatigue life prediction for wheels by simulation of the rotating bending test, *SAE-900147* (1990).

[4] M. Riesner and R. I. DeVries, Finite element analysis and structural optimization of vehicle wheels, *SAE-830133* (1983).

[5] P. R. Raju, B. Satyanarayana, K. Ramji and K. S. Babu, Evaluation of fatigue life of aluminum alloy wheels under radial loads, *Engineering Failure Analysis*, 14 (2007) 791-800.

[6] M. Cerit, Numerical simulation of dynamic side impact test for an aluminum alloy wheel, *Scientific Research and Essays*, 5 (2010) 2694-2701.

[7] C. L. Chang and S. H. Yang, Simulation of wheel impact test using finite element method, *Engineering Failure Analysis*, 16 (2009) 1711-1719.

[8] X. Yuan, L. Zhang, X. Chen, B. Du, B. Li, L. Fan and Y. Pan, Numerical simulation of aluminum alloy wheel 13° im-

pact test based on Abaqus, *Applied Mechanics and Materials*, 215-216 (2012) 1191-1196.
[9] Y. Zheng, B. Li and Z. Wang, Dynamic simulation on impact test of vehicle wheel, *Advanced Engineering Forum*, 2-3 (2012) 890-893.
[10] J. H. Bae, K. C. Jung, S. H. Yoo, S. H. Chang, M. Kim and T. Lim, Design and fabrication of a metal–composite hybrid wheel with a friction damping layer for enhancement of ride comfort, *Composite Structures*, 133 (2015) 576-584.
[11] SAE J175, *Wheels-impact test procedures-road vehicles*, Warrendale (PA), Society of Automotive Engineers, Inc. (2001).
[12] S. F. Hwang and H. T. Liu, Prediction of elastic constants of carbon fabric/polyurethane composites, *Solid State Phenomena*, 258 (2017) 233-236.

Shun-Fa Hwang received his Ph.D. degree in mechanical engineering from the University of California, Los Angeles, USA in 1992 and then joined the Faculty of Mechanical Engineering Department, National Yunlin University of Science and Technology, Taiwan. He was promoted as a Full Professor in 2001. His current interests are composite structure design, digital image correlation, and vibration and sound.